Supplementary Information

Induced Fit and Mobility of Cycloalkanes within Nanometer-sized Confinements at 5K

Aisha Ahsan[a*], Luiza Buimaga-Iarinca[b], Thomas Nijs[a], Sylwia Nowakowska[a], Rejaul Sk[a], S. Fatemeh Mousavi[a], Mehdi Heydari[c], Meike Stöhr[d], Sameena S. Zaman[e], Cristian Morari[b], Lutz H. Gade[f*], Thomas A. Jung[c*]

[a]Dr. A. Ahsan, Dr. S. F. Mousavi, Dr. T. Nijs, Dr. S. Nowakowska, Dr. Rejaul Sk

Department of Physics, University of Basel, Klingelbergstrasse 82, 4056 Basel, Switzerland, E-mail: aisha.ahsan@unibas.ch

[b]Dr. L.Buimaga- Iarinca, Dr. C. Morari

CETATEA, National Institute for Research and Development of Isotopic and Molecular Technologies, 67-103 Donat, 400293 Cluj-Napoca, Romania, E-mail: luiza.iarinca@itim-cj.ro; cristian.morari@itim-cj.ro

[c]Prof. T. A. Jung, M. Heydari

Laboratory for X-ray Nanoscience and Technologies, Paul Scherrer Institut, 5232 Villigen, PSI, Switzerland

E-mail: thomas.jung@psi.ch

[d]Prof. M. Stöhr

Zernike Institute for Advanced Materials, University of Groningen, Nijenborgh 4, 9747 AG Groningen, The Netherlands, E-mail: m.a.stohr@rug.nl

[e]Dr. S. S. Zaman

Habib University, Block 18, Gulistan-e-Jauhar, University Avenue, Off Shahrah-e-Faisal Rd, Karachi-75290, Sindh, Pakistan, E-mail: sameena.shahzaman@sse.habib.edu.pk

[f]Prof. L. H. Gade

Anorganisch-Chemisches Institut, Universität Heidelberg, Im Neuenheimer Feld 270, 69120 Heidelberg, Germany, E-mail: lutz.gade@uni-hd.de

Contents

1. Molecule-by-molecule condensation of c-alkanes.

Samples covered in part by DPDI networks have been exposed to different cyclo-alkanes and investigated by STM. The complete data set showing all observed configurations of **c5** to **c8** in the pores is shown here (Figure S1.1). The cyclo-octane molecules in the situation 4a in Figure S1.1 are mobile within the pore and their average residence time has been estimated from the streak dimensions in cross sections of the STM data. From the timing of the scanlines and the length of the streaks, we estimate an average residence time of the order of ~60 msec. The **c8** case is extraordinary in multiple aspects, (i) as the threefold symmetry of the network is broken by the asymmetric triangle / rectangular arrangement formed at occ(3) and occ(4) respectively and also (ii) in the considerable mobility of the molecules as indicated by the noise in the scanlines. This level of mobility is unexpected at 4K and specifically occurs in the pore, not for c-octanes adsorbed on the metal terrace.

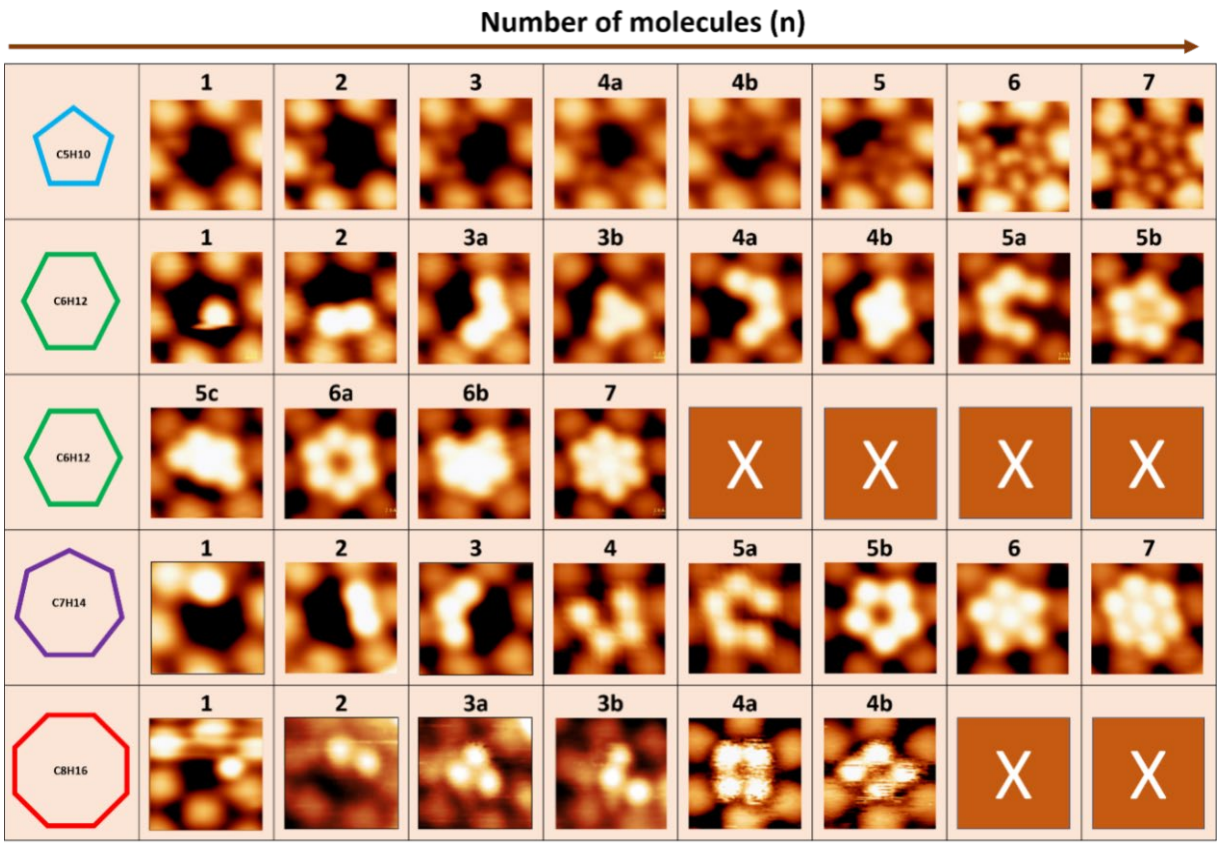

Figure S1: Molecule by molecule condensation of c-alkanes inside confinements. STM images (2.4nm x 2.4nm) of pores containing different number of c-alkane molecules. The pictogram at the left side labels the concerned c-alkane and the number of molecules / pore is indicated by the numbers (n:1-7) above each image where 'a' and 'b' denote condensates comprising the same number of molecules in different configurations as identified from time lapse images. STM parameters: 1V, 6pA, image size: 2.4 nm x 2.4 nm, 256 pixels per frame, scan speed 2nm/sec.

2. Molecular adsorption / condensation statistics

To assess the adsorption / condensation statistics, the relative adsorption in 'network pores' vs the total adsorption on the surface has been tabulated at the bottom of Figure S2. In analogy to the *Langmuir Adsorption Model,* we can take this as an evidence that the adsorption probability for c-alkanes to adsorb in the DPDI pores is significantly higher for **c5** & **c7** (0.79 & 0.76) in comparison to **c6** (0.62). Most remarkably, **c8** shows the least tendency of adsorbing inside the pores (0.07). This non-linear behaviour with the order number and size of the c-alkane is related to the combined effect of spatial confinement and interaction with the quantum well state as explained in the main manuscript.

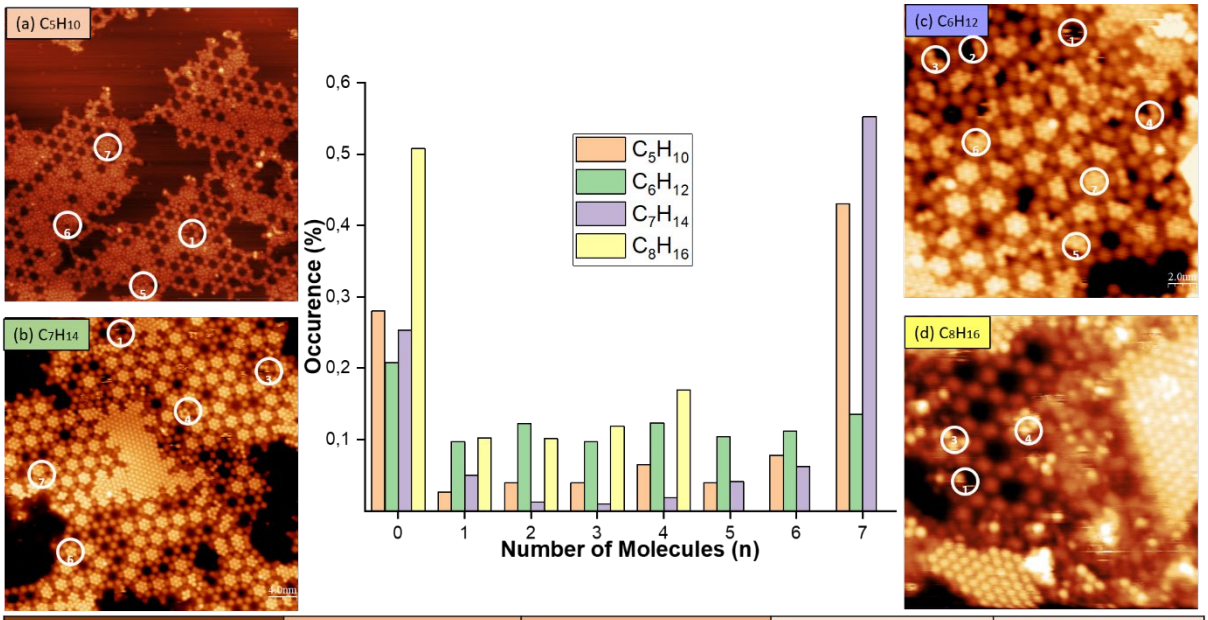

C_xH_{2x}	C_5H_{10}	C_7H_{14}	C_6H_{12}	C_8H_{16}
θ_A = Np / Nt	0.79	0.76	0.62	0.07

Figure S2.1: Histogram analysis of c-alkanes inside DPDI confinements. (a – d) STM micrographs indicating the considerably different adsorption statistics of the investigated c-alkanes in the DPDI network. All samples have been held at 9K while being exposed to 120L c-alkane gas. After exposure, samples have been annealed to 20K and imaged by STM. Around 600 pores have been analysed from different large scale STM micrographs for each of the c-alkanes. Before exposure, all samples have been covered by DPDI network islands covering ~70 % of the surface area. Molecules inside the pores and on the free metal surface can be discriminated by their position with respect to the darker network backbone. The statistical distribution of filled and empty pores strongly depends on the particular cycloalkane and is presented in the centre of the figure as histogram plot. The fractional occupancy (θ_A= N_p / N_t) is tabulated at the bottom of the figure (N_t: total number of molecules counted; N_p: number of molecules adsorbed in the pores). The fractional occupancy θ_A is considerably lower for the largest c-alkane i.e. **c8** than for the other investigated c-alkanes.

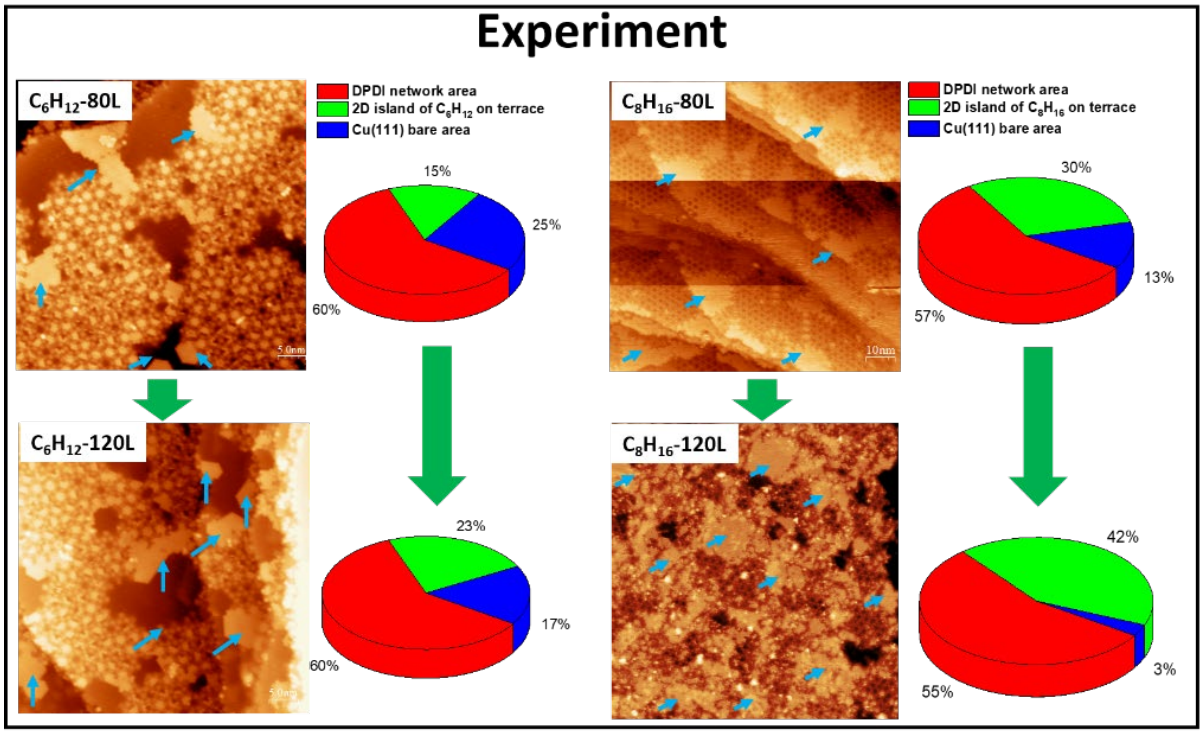

Figure S2.2: Coverage dependent distribution of c-alkanes on network covered and network free area. Left hand side: surface coverage after 80L and 120L exposure of **c6**. The molecular coverage on the network-free, bare Cu(111) terrace increases gradually as exposure time increases. In the STM micrographs for **c6**, a large percentage of the pores is at least partially occupied, even after the lower exposure. Right hand side: surface coverage at 80L and 120L exposure of **c8.** Interestingly the surface coverage of **c8** on bare Cu(111) terraces is comparably high and accompanied by a low fraction of at least partially occupied pores of the network. This data set and histogram analysis indicate that the sticking / adsorption events in the DPDI pores are reduced with increased molecular dimensions. During the deposition process, **c8** relocates from network covered areas to the free Cu surface. Note that the fraction of DPDI network on the samples has been held approximately constant to allow for a valid comparison. Blue arrows in the micrographs indicate the bare Cu(111) surface fraction.

3. Height analysis of c-alkanes inside pores and on bare Cu

Different apparent height analyses of c-alkanes inside confinements are provided in comparison to their apparent height upon adsorption on the network free area are presented in Figure S3.1. The apparent height is shown to depend on both, the position and arrangement of c-alkanes in individual pores (Figure S3.1, top panel outlined in black) and can be referenced to the apparent height of the DPDI network backbone (Figure S3.1, center panel outlined in green). Also, there is a change in the apparent height depending on whether the molecules are adsorbed inside the pores or on the network free terraces (Figure S3.2).

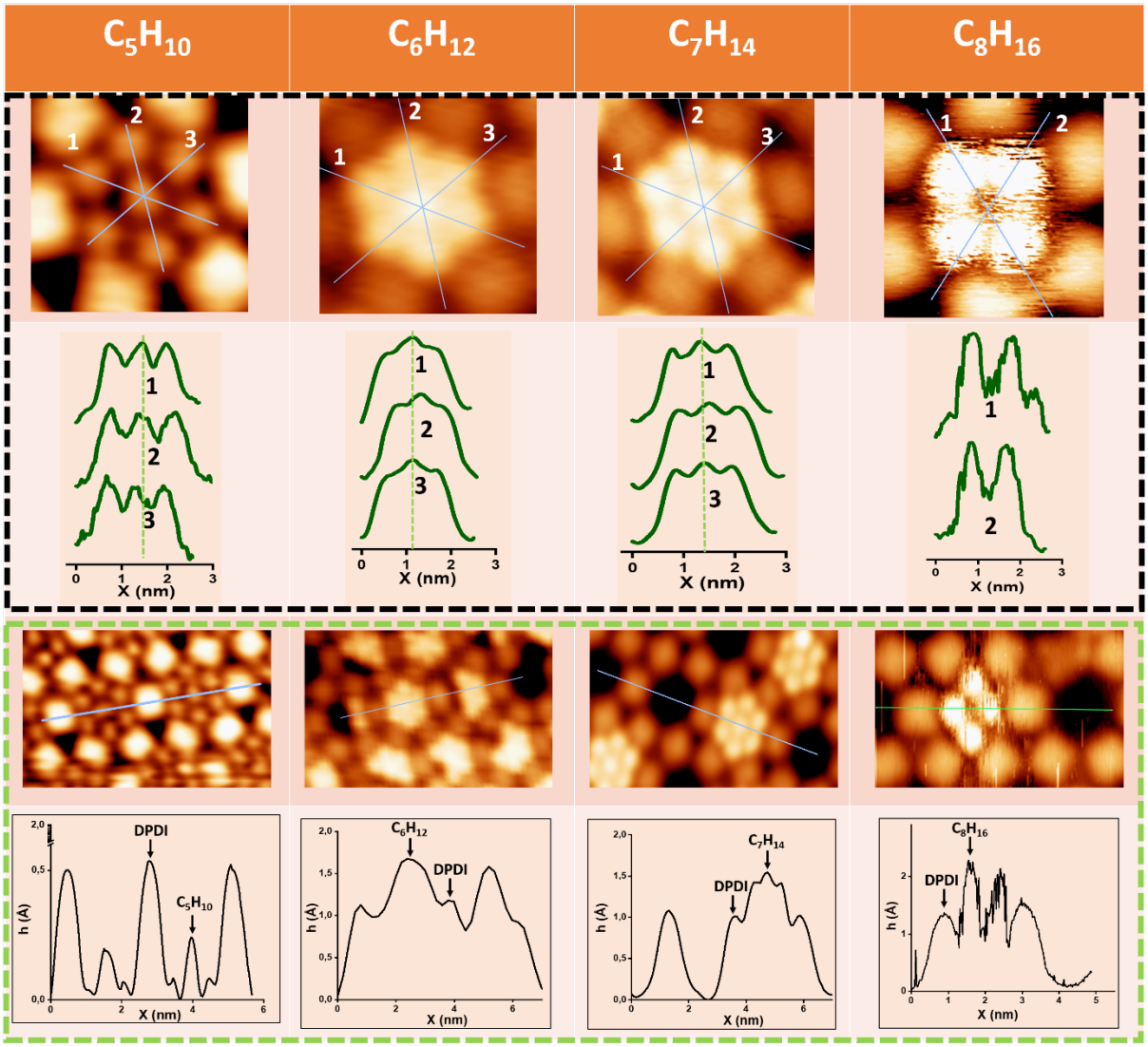

Molecule	h_1 , h_0 (Å)	h_2 , h_0 (Å)	h_3 , h_0 (Å)	h_4 , h_0 (Å)	h_5 , h_0 (Å)	h_6 , h_0 (Å)	h_7 , h_0 (Å)
C_5H_{10}	0.22 , **0.51**	0.21 , **0.50**	0.21 , **0.50**	0.21 , **0.50**	0.22 , **0.51**	0.22 , **0.51**	0.24 , **0.53**
C_6H_{12}	1.28 , **0.95**	1.26 , **0.91**	1.38 , **1.00**	1.45 , **1.08**	1.53 , **1.15**	1.55 , **1.21**	1.67 , **1.18**
C_7H_{14}	1.36 , **0.91**	1.36 , **0.90**	1.38 , **0.90**	1.39, **0.92**	1.43 , **0.96**	1.40 , **0.90**	1.54 , **1.01**
C_8H_{16}	2.03 , **1.45**	2.01 , **1.43**	2.02 , **1.43**	2.21 , **1.59**	Xxx	xxx	xxx

Molecule	(h_1-h_0) (Å)	h_1/h_0	(h_2-h_0) (Å)	h_2/h_0	(h_3-h_0) (Å)	h_3/h_0	(h_4-h_0) (Å)	h_4/h_0	(h_5-h_0) (Å)	h_5/h_0	(h_6-h_0) (Å)	h_6/h_0	(h_7-h_0) (Å)	h_7/h_0
C_5H_{10}	-0.28	0.43	-0.29	0.42	-0.29	0.42	-0.29	0.42	-0.29	0.43	-0.29	0.43	-0.29	0.45
C_6H_{12}	0.34	1.35	0.35	1.38	0.38	1.38	0.37	1.34	0.38	1.33	0.34	1.28	0.49	1.42
C_7H_{14}	0.45	1.49	0.46	1.51	0.48	1.53	0.47	1.51	0.47	1.49	0.50	1.56	0.53	1.52
C_8H_{16}	0.58	1.4	0.58	1.41	0.59	1.41	0.62	1.39						

Figure S3.1: Apparent STM height: profile analysis of c-alkanes in the DPDI confinements. Three panels have been compiled with STM data and simulations which are: i) position dependent apparent STM height of c-alkanes inside pores (*black outlined table*), ii) the relative height of c-alkanes with respect to the DPDI network backbone (*green outlined table*) and iii) the occupancy dependent evolution of the apparent height (*red outlined table*). *Black table:* STM micrographs of the completely c-alkane-filled pores are shown at the top. The in-pore intermolecular distances between the individual

molecules and the apparent STM height can be analysed from the cross sections shown below the STM micrographs. Note that the center molecule for **c6** and **c7** in the fully occupied pores is protruding slightly higher than its six neighbours. This is an effect which we tentatively associate with steric constraints upon full packing of the pore. *Green table:* The apparent height of c-alkanes within the pores in comparison to the DPDI network backbone is characteristically different for **c5** and **c6-c8** as it can be recognized in the STM micrographs and cross sections. *Red table:* All determined height parameters have been provided and compared as they are discussed in the main manuscript; absolute and relative comparisons are listed. The difference between the height of the molecules at occupancy occ(i) is tabulated as h_i and the height of the DPDI is tabulate as h_0. All values are given in Å. STM parameters: 1V, 6pA, pixels per frame: 256 px, scan speed 2nm/sec.

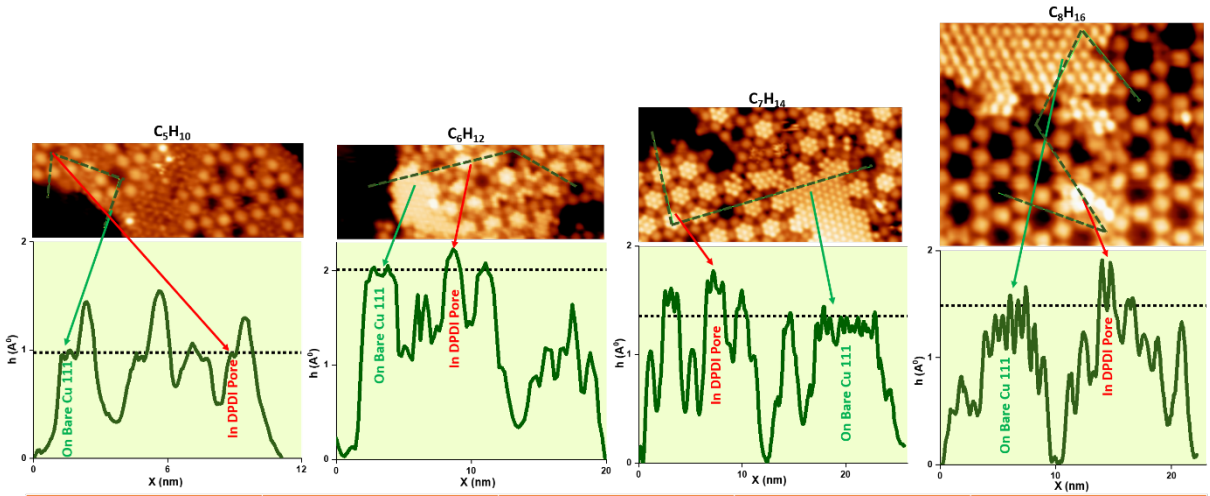

Molecule	C_5H_{10}	C_6H_{12}	C_7H_{14}	C_8H_{16}
$(h_p\text{-}h_t)^{DFT}$	0.4	0.22	0.27	0.21
$(h_{p(full)}\text{-}h_t)^{EXP}$	0.01	0.24	0.33	0.52

Figure S3.2: Apparent STM height profile analysis of c-alkanes in fully filled DPDI pores in comparison with supramolecular islands on bare Cu(111). The STM apparent height of the fully occupied pore, $\mathbf{h_{p(full)}}$ has been compared to the corresponding height of extended 2D islands on neighbouring terraces $\mathbf{h_t}$. The apparent height differences increase monotonously from **c5** to **c8** indicating an increasingly strong site-specific interaction inside the pore. This trend is well captured in the DFT calculations (row labelled with $\mathbf{(h_p\text{-}h_t)^{DFT}}$ in the table at the bottom of the figure) with the increase towards **c8** being lower than experimentally observed. We tentatively assign this exception to the experimentally observed dynamicity of **c8** on the time scale of ~60 msec which may not be captured by DFT in a straightforward way. Note that the data in the table has been obtained from a small number (~3-5) of representative cross sections taken at different places across the sample. STM parameters: 1V, 6pA.

c5 exhibits an exceptionally low apparent height of ~ 43% of the apparent height of the DPDI backbone (Figure S3.1). The close contact between **c5** at full (occ-7) occupancy of the pore may also cause the interesting trapezoidal shape of the center molecule in the STM micrographs (Figure S3.1 top right). In the experiment, the higher order number c-alkanes **c6 – c8** exhibit a considerably larger apparent height, higher than the DPDI backbone (Further details of the apparent height analysis are tabulated in Figure S3.1 & Figure S3.2).

4. DFT Estimate of binding energy of c-alkanes in pores

Conformer	ΔE_0	ΔE^1_P	$\Delta E^2_P/2$
C_5H_{10}	-0.47	-0.67	-0.57
C_6H_{12}	-0.49	-0.67	-0.59
C_7H_{14}	-0.61	-0.74	-0.70
C_8H_{16}	-0.66	-0.79	-0.74

Figure S4: **Binding energy of cyclo-alkanes in pores: decreasing energy per molecule with occupancy increasing from 1 to 2.** The binding energy is given in eV; ΔE_0 is binding energy on bare surface while ΔE^n_P (n = 1, 2) is the binding energy inside pore for single (n=1) or two (n=2) molecules. Note that DFT only captures the Energy ground state which in conjunction with the observed phenomena may not be the relevant state, in particular at higher packing density.

5. Pauli repulsion between confined surface state and the c-alkanes

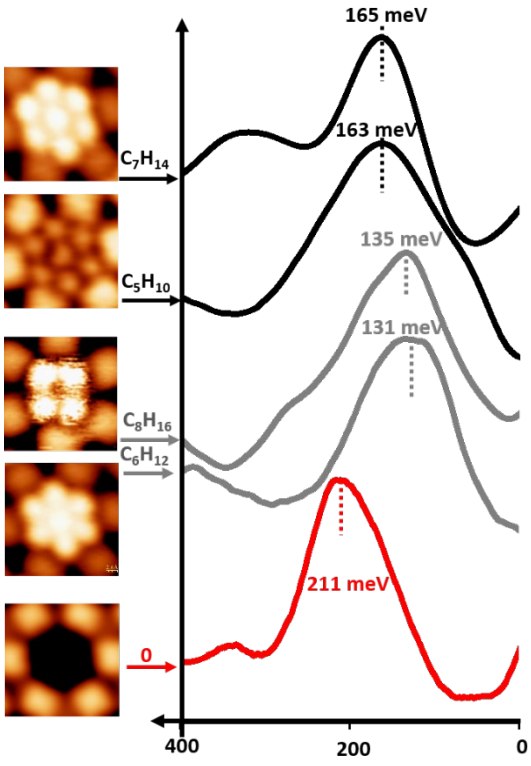

Figure S5: Pauli Repulsion: Fully filled c-alkanes interacting with the confined surface state. Comparing the Pauli repulsion, the c-alkanes containing an uneven number of C-atoms (**c5** and **c7**) exhibit a binding energy (BE) shift which is ~30 meV closer to the BE of the native confined surface

state (CSS) (lower Pauli repulsion, more relaxed) than their even order number counterparts **c6** and **c8**. This is taken as a sign for the changing adsorption mode as discussed in the main paper.

6. C-alkane conformation on Cu(111)

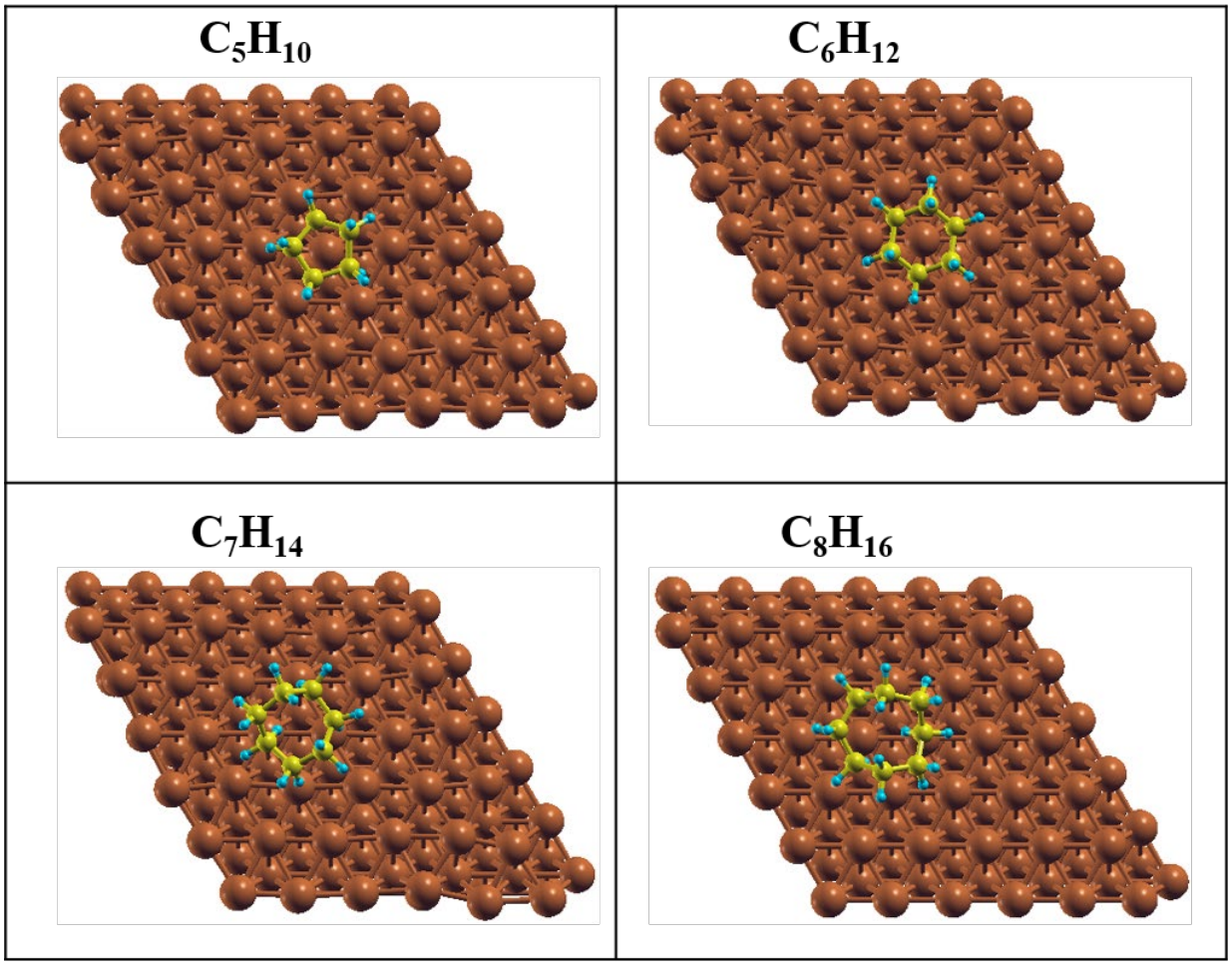

Figure S6: **c-alkanes after relaxation on Cu(111).** 3D plots of the atomic structures obtained with the DFT calculations presented in Table 1 of the main paper. *Top-left*: the lowest energy configuration of C_5H_{10} on Cu(111) is close to the envelope configuration which is degenerate in that each C-atom can take the role of the 'flap'. *Bottom-left*: C_7H_{14} assumes a less close to planar configuration suggesting that the stabilization via the surface is less effective. *Second column*: C_6H_{12} adsorbs in an only slightly closer to planar chair configuration and C_8H_{16} assumes a complex shape which is again less coplanar with the surface. The decreased planarity of molecular module facilitates a lower adsorption energy and residual dynamicity compared to planar or strongly interacting molecules. (see also Table 1 in main paper)

7. Bond length comparison of c-alkanes.

For free molecules (i.e. no influence of the surface) we see that almost all bonds share the same length, close to 1.12 Angstroms as shown in (Figure S-7). For the molecules adsorbed on clean Cu(111) surface (yellow plots) **c5**, **c6** and **c7** have a clear tendency to increase their C-H bond lengths (i.e. the C-H bond is stretched by the forces acting in the surface potential). For **c8**, we note both shorter and longer C-H bonds. This indicates, that the interaction of **c8** with the surface is different from the other three cases. Finally, upon adsorption of the c-alkanes in the pore, the situation becomes much more complex, with shorter C-H bonds for **c5** and mixtures of shorter/longer bonds for the other molecules. Nevertheless, the plot suggests a trend to form shorter C-H, indicating that its interaction with the surface is different from the other three. While the changes in the C-H lengths are relatively small, the trends are sufficiently clear to conclude that the interaction between molecules and clean surface is different from that between molecule and the surface state inside the pore. Indeed, the surface state leads to a shift of the Fermi level which in turn influences the molecule-surface charge transfer / interaction mechanisms. This has two reasons; (1) changes in the line-up of the Fermi level, and (2) the position of molecular HOMO/LUMO. An inspection of the aforementioned data shows that this effect is very weak for **c8** while it is maximum for the **c6**. Note that this simulation has only been performed for a few molecules inside the pores. Therefore, it is indicative of the complexity of the mechanisms involved in the process, but not a realistic representation of the experimental situation. The observed changes in the simulation are strongly suggesting that upon pore filling similar bond-length and bond angle, modifications occur as they are expected to cause the phenomena as they are explained by the ‘induced fit’ concept in the main paper.

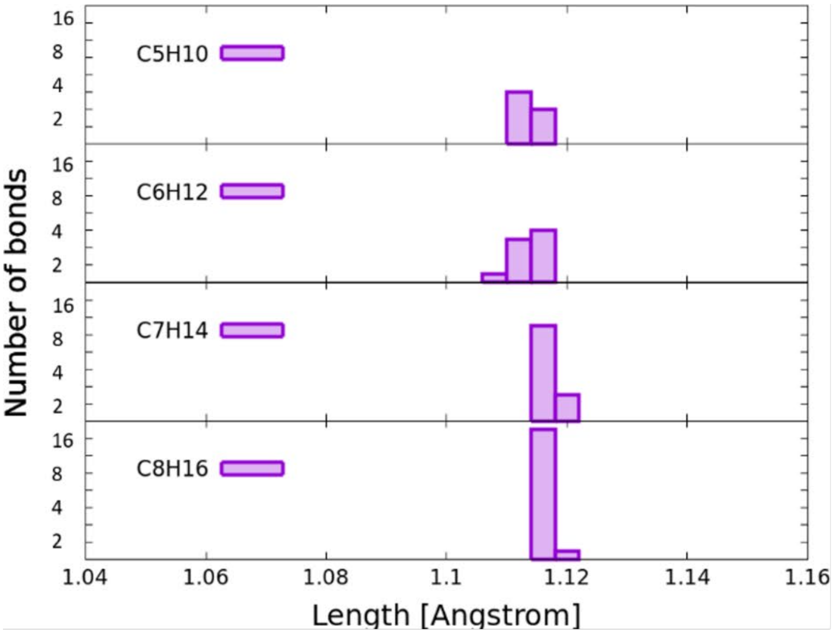
C5H10
C6H12
C7H14
C8H16
Number of bonds
16
8
4
2
1.04
1.06
1.08
1.1
1.12
1.14
1.16
Length [Angstrom]

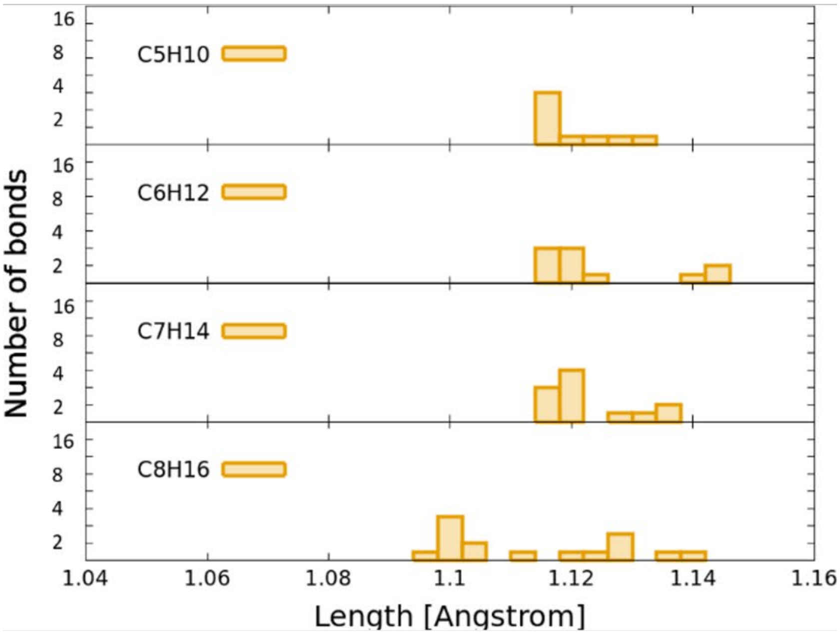
C5H10
C6H12
C7H14
C8H16
Number of bonds
16
8
4
2
1.04
1.06
1.08
1.1
1.12
1.14
1.16
Length [Angstrom]

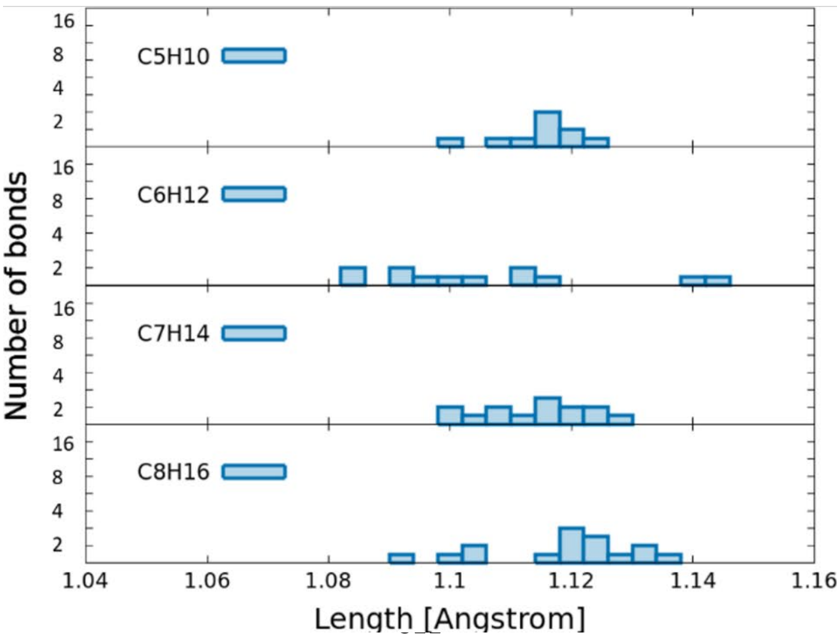
C5H10
C6H12
C7H14
C8H16
Number of bonds
16
8
4
2
1.04
1.06
1.08
1.1
1.12
1.14
1.16
Length [Angstrom]

Figure S7. Graphical representation of the C-H bond-lengths for the free molecules (purple), modified by their adsorption in supramolecular islands on Cu(111) (yellow) and by their adsorption inside the pore (blue). The histogram nicely reflects the uniform bond length for the minimal energy conformation in vacuum, the bond length spreading by the molecule-surface interaction in the contact zone leading to unequal bond extension. In the third case the Pauli interaction with the confined surface state 'softens' the hard sphere interaction of the contact atoms with the adsorbate and therefore an in-between position is assumed between the in-vacuum (relaxed) and the on-surface (bottom side supported) conformations and bond length spectra. Each bar shows the number of C-H bonds with a certain length, starting from the value of 1.04 Angstroms, with a step size of 0.03 Angstroms.

8. Methods

Sample preparation and STM measurement:

The samples have been prepared and examined in an ultrahigh vacuum (UHV) system with a base pressure of 6 x 10^{-11} mbar. The Cu(111) crystal (MaTecK GmbH) has been prepared by rounds of Ar^+ sputtering at E = 1 keV performed at room temperature followed by annealing at 480 ºC. The DPDI molecules have been deposited from a nine-cell commercial evaporator (Kentax, GmbH, Germany) on the Cu(111) by sublimation at ~240 ºC and the rate has been controlled before deposition by a quartz crystal microbalance. After deposition, the sample has been annealed to 290-300 ºC in order to convert DPDI into 3deh-DPDI, which crafts the Cu-coordinated network. Cycloalkanes of purity 99% has been cleaned from air contamination by freeze – pump – thaw – cycles. A leak valve equipped with a capillary has been used to direct the molecular vapour closer (~20 cm) to the sample in the STM setup. Thus, contamination of the cryogenic system shields by the dosing experiments has been reduced. During the dosing procedure, the STM tip had been visibly retracted (~ 100 micrometer) from the surface. The STM has been operated at the equilibration temperature of the He bath cryostate (4.2K). By opening of the cryo-shields during the molecular deposition process, the T reference measurement increased up to ~5.5 K. All STM data presented in Figure1-Figure 4 (main paper) and in Figure S1-S5 have been acquired after exposure of the Cu-coordinated 3deh-DPDI network to 120 L to the corresponding cycloalkanes. During the exposure an overall chamber pressure equal to 1.3 x 10^{-7} mbar has been measured. 1,200 s was the typical during exposure time for the samples held at ~9 K. After exposure with corresponding c-alkanes, samples were annealed upto 20K. The STM was operated after pumping down to the base pressure and with closed cryoshields in the He cryostat (~4.2K).

STM measurements have been performed in the constant current mode with Pt–Ir tips (90% Pt, 10% Ir). The tip has been prepared by mechanical cutting followed by sputtering and controlled indentation into bare Cu(111) surfaces. If not specified differently, 1V sample bias has been applied and the feedback circuit has been set to a tunnelling current of 6pA.

DFT computational setup

Simulations were performed using the SIESTA code[1,2]. As exchange-correlation functional, we have used the vdW-DF-cx functional of Berland and Hyldgaard (BH)[3]. The advantage of

this functional over other van der Waals functionals is that it accurately reproduces the structure of the metallic bulk. By calculating crystalline Cu we obtain a lattice constant of 3.64 Å; this comprises a value 0.8% difference than experimental value (3.61 Å). As basis sets, we used double-zeta polarized (DZP) with an energy shift of 50 meV for Cu slab, while for the cycloalkanes we have used triple-zeta polarized basis sets (TZP) with an energy shift of 25 meV.

The geometry used for the surface decorated with DPDI pores is that reported by Matena et al; [4] to simulate the copper surface we used 4 atomic layers, passivated by a layer of H and accommodated into a 10x10 supercell on the Cu(111) surface. 6x6 super-cell dimensions have been chosen for calculations on the bare surface in absence of the network. The length of the cells along the OZ axis was 40 Å for all systems, thus permitting a vacuum level of ≈ 30 Å and allowing us to avoid the artificial influence of the electric charge from one cell to another.

For all the systems, we calculated Gamma point integrals in the Brillouin zone. Structural relaxation was undertaken in two steps; in order to assess the molecule's intrinsic flexibility, we have used the 'simulated annealing' method with an initial temperature T=500K and a final annealing temperature of 2K. The time step of the dynamics in the sequences was 1 fs. Next, the systems were minimized until the maximum gradient in the relaxed structure was below 0.01 eV/Å by using the Conjugated Gradient algorithm.

Simulated STM images have been obtained by using the Tersoff-Hamman approximation[5] as implemented by Lorente and Persson[6]. We computed the STM images for a bias of 1 V in a simulation of a 'constant current' STM experiment (i.e. following a constant value of local density of states in Tersoff Hamman approximation).

We have performed structural relaxation for all relevant conformers reported in the literature in order to assess the validity of our methods. Our results are in accord to those already reported [c5-c8][7–10].

REFERENCES

(1) Ordejón, P.; Artacho, E.; Soler, J. M. Self-Consistent Order- N Density-Functional Calculations for Very Large Systems. *Phys. Rev. B* **1996**, *53* (16), R10441–R10444.

(2) Soler, J. M.; Artacho, E.; Gale, J. D.; García, A.; Junquera, J.; Ordejón, P.; Sánchez-Portal, D. The SIESTA Method for *Ab Initio* Order- *N* Materials Simulation. *J. Phys. Condens. Matter* **2002**, *14* (11), 2745–2779.

(3) Berland, K.; Hyldgaard, P. Exchange Functional That Tests the Robustness of the Plasmon Description of the van Der Waals Density Functional. *Phys. Rev. B* **2014**, *89* (3), 035412.

(4) Matena, M.; Björk, J.; Wahl, M.; Lee, T.-L.; Zegenhagen, J.; Gade, L. H.; Jung, T. A.; Persson, M.; Stöhr, M. On-Surface Synthesis of a Two-Dimensional Porous Coordination Network: Unraveling Adsorbate Interactions. *Phys. Rev. B* **2014**, *90* (12), 125408.

(5) Tersoff, J.; Hamann, D. R. Theory of the Scanning Tunneling Microscope. *Phys. Rev. B* **1985**, *31* (2), 805–813.

(6) Lorente, N.; Persson, M. Theoretical Aspects of Tunneling-Current-Induced Bond Excitation and Breaking at Surfaces. *Faraday Discuss.* **2000**, *117*, 277–290.

(7) Ocola, E. J.; Bauman, L. E.; Laane, J. Vibrational Spectra and Structure of Cyclopentane and Its Isotopomers. *J. Phys. Chem. A* **2011**, *115* (24), 6531–6542.
(8) Tekautz, G.; Binter, A.; Hassler, K.; Flock, M. Chair, Boat and Twist Conformation of Dodecamethylcyclohexasilane and Undecamethylcyclohexasilane: A Combined DFT and Raman Spectroscopic Study. *ChemPhysChem* **2006**, *7* (2), 421–429.
(9) Freeman, F.; Hwang, J. H.; Hae Junge, E.; Dinesh Parmar, P.; Renz, Z.; Trinh, J. Conformational Analysis of Cycloheptane, Oxacycloheptane, 1,2-Dioxacycloheptane, 1,3-Dioxacycloheptane, and 1,4-Dioxacycloheptane: Conformational Analysis of Oxacycloheptanes. *Int. J. Quantum Chem.* **2008**, *108* (2), 339–350.
(10) Rocha, W. R.; Pliego, J. R.; Resende, S. M.; Dos Santos, H. F.; De Oliveira, M. A.; De Almeida, W. B. Ab Initio Conformational Analysis of Cyclooctane Molecule. *J. Comput. Chem.* **1998**, *19* (5), 524–534.